

Gas-liquid interface treatment in underwater explosion problem using moving least squares-smoothed particle hydrodynamics

Gaku Hashimoto*

RIKEN, 2-1 Hirosawa, Wako-shi, Saitama 351-0198, Japan

Hirohisa Noguchi‡

Keio University, 3-14-1 Hiyoshi, Kohoku-ku, Yokohama-shi, Kanagawa 223-8522, Japan

(Received September 10, 2007, Accepted May 12, 2008)

Abstract. In this study, we investigate the discontinuous-derivative treatment at the gas-liquid interface in underwater explosion (UNDEX) problems by using the Moving Least Squares-Smoothed Particle Hydrodynamics (MLS-SPH) method, which is known as one of the particle methods suitable for problems where large deformation and inhomogeneity occur in the whole domain. Because the numerical oscillation of pressure arises from derivative discontinuity in the UNDEX analysis using the standard SPH method, the MLS shape function with Discontinuous-derivative Basis Function (DBF) that is able to represent the derivative discontinuity of field function is utilized in the MLS-SPH formulation in order to suppress the nonphysical pressure oscillation. The effectiveness of the MLS-SPH with DBF is demonstrated in comparison with the standard SPH and conventional MLS-SPH through a shock tube problem and benchmark standard problems of UNDEX of a trinitrotoluene (TNT) charge.

Keywords: gas-liquid interface; discontinuous derivative; underwater explosion; smoothed particle hydrodynamics; moving least squares.

1. Introduction

High accurate analyses of mechanical interaction between different phases, for example, fluid-structure interaction (FSI), soil-structure interaction, two-phase flow, interfacial behavior of a composite material, tool-rock interaction, etc., are important research subjects in order to elucidate complex physical phenomena. In recent years, various simulation approaches have been developed and applied for each interaction analysis (see de Borst *et al.* 2008, Jahromi *et al.* 2008, Rojek and Oñate 2008). The present paper focuses on gas-liquid phase flow problems, especially underwater explosion (UNDEX) problems. The UNDEX is caused by the detonation of a high explosive charge. First the detonation-produced explosive gas expands into the surrounding water. Then underwater shock wave arises and propagates in the water. Finally the underwater shock wave

* E-mail: gashimoto@riken.jp

‡ E-mail: noguchi@sd.keio.ac.jp

interacts with the nearby structure. It is very difficult to implement mesh-based method to analyze the UNDEX problem because large deformation and inhomogeneity occur in the whole analysis domain (see Liu and Liu 2003). On the other hand, the particle-based Smoothed Particle Hydrodynamics (SPH) method by Lucy (1977) and Gingold and Monaghan (1977) has been applied to UNDEX problems and its effectiveness has been shown by Liu *et al.* (2002), Liu *et al.* (2003) and Kobashi and Matsuo (2005). However, the standard SPH method has two serious problems. Firstly, the standard SPH method does not guarantee consistency when reproducing a polynomial function. This often results in a severe accuracy reduction due to the boundary deficiency or unbalanced particle distribution in a support domain (see Liu and Liu 2003). Secondly, when using the SPH method to analyze UNDEX problems, numerical pressure oscillation arises in the domain close to the gas-liquid interface. This oscillation is caused by the discontinuous derivative of pressure at the gas-liquid interface.

In this study, the Moving Least Squares-Smoothed Particle Hydrodynamics (MLS-SPH) method originally proposed in Dilts (1999, 2000) is applied to analyze UNDEX problems. The MLS approximation can be found in Lancaster (1981) and is often used as an approximation in meshfree methods, such as Element-free Galerkin (EFG) method by Belytschko *et al.* (1994). The MLS approximation with a linear basis function has 1st order consistency that is not always maintained in the standard SPH method. In addition, Discontinuous-derivative Basis Function (DBF) by Masuda and Noguchi (2006) is employed to introduce derivative discontinuity to the MLS approximation. Although the normal velocity and the pressure are initially discontinuous on the gas-liquid interface, they become continuous and only their derivatives become discontinuous when the expansion process of gas begins. Therefore it is effective to use the MLS approximation with DBF that is able to express derivative discontinuity of the physical quantities at the gas-liquid interface.

On the other hand, in order to deal with shock waves, Liu *et al.* (2003) proposed using the Discontinuous SPH (DSPH) method, which was developed from the basis of Corrective Smoothed Particle Method (CSPM) by Chen, Beraun and Carney (1999). The Taylor series expansion in the piecewise continuous subdomains on both sides of discontinuity is utilized in the formulation. Liu *et al.* verified the effectiveness in one-dimensional shock problems, such as shock tube and trinitrotoluene (TNT) slab detonation. However the extension to two-dimensional or three-dimensional problems was referred as a future work and has not been seen yet.

This paper is organized as follows: In Chapter 2, the governing equations for inviscid and adiabatic flow are described. In Chapter 3, the MLS approximation with DBF is introduced briefly along with the conventional approximation. It is also demonstrated that the MLS with DBF has a remarkable capacity for reproducing a field function with derivative-discontinuity. In Chapter 4, the MLS-SPH formulation and the leap-frog time marching are given. In Chapter 5, we deal with one-dimensional shock tube problem to examine application of the DBF to the domain close to the contact discontinuity of ideal gas. Though the velocity and the pressure are discontinuous at the contact discontinuous face initially, only the derivatives become discontinuous as well as in the gas-liquid interface case after the computation starts. In Chapter 6, we analyze one-dimensional UNDEX of a TNT slab charge and two-dimensional UNDEX of a square TNT charge in a rigid container to investigate the application of DBF to the domain near the gas-liquid interface. Finally, This paper is concluded in Chapter 7.

2. Governing equations

The fluid is assumed to be inviscid and adiabatic. The conservation laws of mass, momentum and internal energy, and the equation of state are written as follows:

Continuity equation:

$$\frac{d\rho}{dt} = -\rho\nabla \cdot \mathbf{v} \quad (1a)$$

Equations of motion:

$$\rho \frac{d\mathbf{v}}{dt} = -\nabla p \quad (1b)$$

Energy Equation:

$$\rho \frac{de}{dt} = -p\nabla \cdot \mathbf{v} \quad (1c)$$

Equation of state:

$$p = p(\rho, e) \quad (1d)$$

where d/dt is the material time-derivative, ρ is the density, ∇ is the gradient operator taken with respect to the spatial coordinates, \mathbf{v} is the velocity, p is the pressure, e is the specific internal energy.

3. MLS approximation

3.1 Conventional MLS approximation

A support domain $\Lambda(\mathbf{x})$ of a field point \mathbf{x} is defined (see Fig. 1 (a)). The conventional MLS approximation can be written as follows:

$$\begin{aligned} u(\mathbf{x}) \approx u_h(\mathbf{x}) &= \sum_{J \in \Lambda(\mathbf{x})} \{w(\mathbf{x} - \mathbf{x}^J, h^J) \mathbf{p}^T(\mathbf{x}) \mathbf{A}^{-1}(\mathbf{x}) \mathbf{p}(\mathbf{x}^J)\} u^J \\ &= \sum_{J \in \Lambda(\mathbf{x})} \phi^J(\mathbf{x}) u^J \end{aligned} \quad (2)$$

where $u(\mathbf{x})$ is the field function, $u_h(\mathbf{x})$ is the approximate field function of $u(\mathbf{x})$, u^J is the value of node J ($J = 1, 2, \dots, N$), \mathbf{x}^J is the coordinates of position vector, h corresponds to the smoothing length in the SPH method, the radius of the influence domain is κh^J , $w(\mathbf{x}, h)$ is the weight function, $\mathbf{p}(\mathbf{x})$ is the polynomial basis vector, $\phi^J(\mathbf{x})$ is the MLS shape function and $\mathbf{A}(\mathbf{x})$ is the moment matrix written as

$$\mathbf{A}(\mathbf{x}) = \sum_{J \in \Lambda(\mathbf{x})} w(\mathbf{x} - \mathbf{x}^J, h^J) \mathbf{p}(\mathbf{x}^J) \mathbf{p}^T(\mathbf{x}^J) \quad (3)$$

The weight function $w(\mathbf{x}, h)$ used in this study is the cubic spline function ($\kappa = 2$) written as

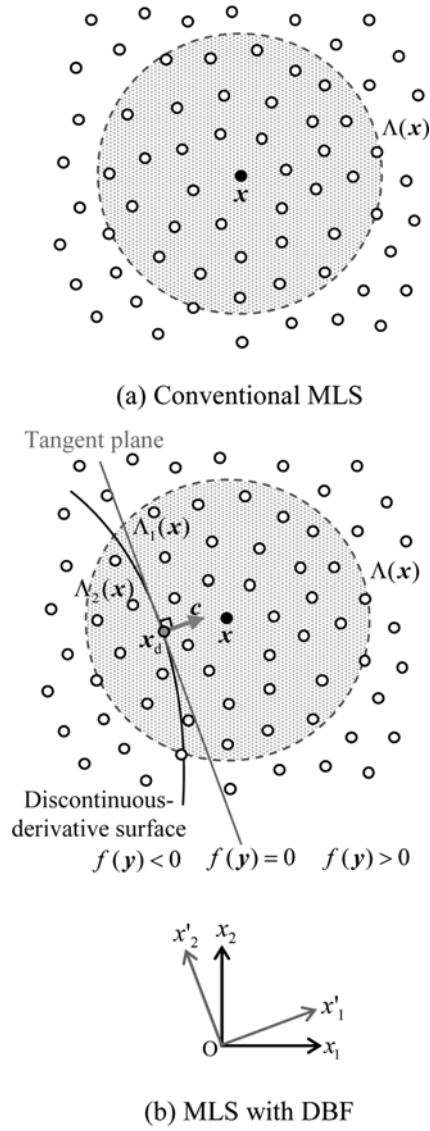


Fig. 1 Support domains for a field point \mathbf{x}

$$w(\mathbf{x}, h) = \begin{cases} \frac{2}{3} - \left(\frac{|\mathbf{x}|}{h}\right)^2 + \frac{1}{2}\left(\frac{|\mathbf{x}|}{h}\right)^3 & \left(\frac{|\mathbf{x}|}{h} \leq 1\right) \\ \frac{1}{6} \left\{ 2 - \left(\frac{|\mathbf{x}|}{h}\right) \right\}^3 & \left(1 < \frac{|\mathbf{x}|}{h} \leq 2\right) \\ 0 & \left(2 < \frac{|\mathbf{x}|}{h}\right) \end{cases} \quad (4)$$

The two-dimensional linear polynomial basis vector is expressed as

$$\mathbf{p}(\mathbf{x}) = \begin{pmatrix} 1 \\ x_1 \\ x_2 \end{pmatrix} \quad (5)$$

Moreover, by using the definition of $\mathbf{b}(\mathbf{x}) = w(\mathbf{x} - \mathbf{x}^J, h^J)\mathbf{p}(\mathbf{x}^J)$ and $\boldsymbol{\gamma}(\mathbf{x}) = \mathbf{A}(\mathbf{x})^{-1}\mathbf{p}(\mathbf{x})$, the x_i -derivative is written as

$$\begin{aligned} \frac{\partial u}{\partial x_i} &\simeq \frac{\partial u_h}{\partial x_i} = \sum_{J \in \Lambda(\mathbf{x})} \left\{ \frac{\partial}{\partial x_i} \boldsymbol{\gamma}^T(\mathbf{x}) \mathbf{b}(\mathbf{x}) + \boldsymbol{\gamma}^T(\mathbf{x}) \frac{\partial}{\partial x_i} \mathbf{b}(\mathbf{x}) \right\} u^J \\ &= \sum_{J \in \Lambda(\mathbf{x})} \frac{\partial \phi^J}{\partial x_i} u^J \end{aligned} \quad (6)$$

3.2 MLS approximation with DBF

The MLS approximation with DBF was initially proposed by Masuda and Noguchi (2006) to express derivative discontinuity. In the paper, solid problems with material discontinuity were analyzed using the EFG method. Fig. 1 (b) shows a discontinuous derivative surface in a support domain $\Lambda(\mathbf{x})$ of a field point \mathbf{x} . \mathbf{x}_d is a point on the surface and the nearest to \mathbf{x} . The tangent plane $f(\mathbf{y})$ at the point \mathbf{x}_d can be defined. By the tangent plane $f(\mathbf{y})$, the support domain $\Lambda(\mathbf{x})$ is divided into two subdomains, $\Lambda_1(\mathbf{x})$ and $\Lambda_2(\mathbf{x})$ defined as

$$f(\mathbf{y}) \geq 0 \quad \text{for } \forall \mathbf{y} \in \Lambda_1(\mathbf{x}) \quad (7a)$$

$$f(\mathbf{y}) < 0 \quad \text{for } \forall \mathbf{y} \in \Lambda_2(\mathbf{x}) \quad (7b)$$

\mathbf{c} is the unit vector normal to the tangent plane $f(\mathbf{y})$ and located at the point \mathbf{x}_d . The tangent plane $f(\mathbf{y})$ can be written as

$$f(\mathbf{y}) = \mathbf{c} \cdot (\mathbf{y} - \mathbf{x}_d) \quad (8)$$

where the unit normal vector \mathbf{c} is always chosen to satisfy the condition as

$$f(\mathbf{x}) = \mathbf{c} \cdot (\mathbf{x} - \mathbf{x}_d) \geq 0 \quad (9)$$

If the function is continuous and the derivative is discontinuous on the tangent plane $f(\mathbf{y})$, two kinds of polynomial basis vectors $\mathbf{p}_1(\mathbf{y})$ and $\mathbf{p}_2(\mathbf{y})$ are used for $f(\mathbf{y}) \geq 0$ and $f(\mathbf{y}) < 0$ respectively in the MLS approximation. These polynomial basis vectors are called Discontinuous-derivative Basis Function (DBF). Then the MLS approximation with DBF can be expressed as follows:

$$\begin{aligned} u(\mathbf{x}) &\simeq u_h(\mathbf{x}) \\ &= \sum_{J \in \Lambda_1(\mathbf{x})} \{ w(\mathbf{x} - \mathbf{x}^J, h^J) \mathbf{p}_1^T(\mathbf{x}) \mathbf{A}^{-1}(\mathbf{x}) \mathbf{p}_1(\mathbf{x}^J) \} u^J \end{aligned}$$

$$\begin{aligned}
& + \sum_{J \in \Lambda_2(x)} \{w(\mathbf{x} - \mathbf{x}^J, h^J) \mathbf{p}_1^\top(\mathbf{x}) \mathbf{A}^{-1}(\mathbf{x}) \mathbf{p}_2(\mathbf{x}^J)\} u^J \\
& = \sum_{J \in \Lambda(x)} \phi^J(\mathbf{x}) u^J
\end{aligned} \tag{10}$$

where the moment matrix $\mathbf{A}(\mathbf{x})$ is

$$\begin{aligned}
\mathbf{A}(\mathbf{x}) & = \sum_{J \in \Lambda_1(x)} w(\mathbf{x} - \mathbf{x}^J, h^J) \mathbf{p}_1(\mathbf{x}^J) \mathbf{p}_1^\top(\mathbf{x}^J) \\
& + \sum_{J \in \Lambda_2(x)} w(\mathbf{x} - \mathbf{x}^J, h^J) \mathbf{p}_2(\mathbf{x}^J) \mathbf{p}_2^\top(\mathbf{x}^J)
\end{aligned} \tag{11}$$

In this study, the transformation of coordinates is utilized in a two-dimensional problem to simplify the algorithm and written as the following equation.

$$\begin{pmatrix} x'_1 \\ x'_2 \end{pmatrix} = \begin{pmatrix} c_1 & c_2 \\ -c_2 & c_1 \end{pmatrix} \begin{pmatrix} x_1 \\ x_2 \end{pmatrix} \tag{12}$$

Then the tangent plane is always expressed as $f(\mathbf{x}) = x'_1 - (x'_d)_1 = 0$ where $(x'_d)_i$ is the x'_i -component of \mathbf{x}'_d , and thus the two-dimensional polynomial basis vectors are written as

$$\mathbf{p}_1(\mathbf{x}) = \begin{pmatrix} 1 \\ x'_1 - (x'_d)_1 \\ x'_2 - (x'_d)_2 \\ 0 \end{pmatrix} \tag{13a}$$

$$\mathbf{p}_2(\mathbf{x}) = \begin{pmatrix} 1 \\ 0 \\ x'_2 - (x'_d)_2 \\ x'_1 - (x'_d)_1 \end{pmatrix} \tag{13b}$$

Similarly, by using the definition of $\mathbf{b}_1(\mathbf{x}) = w(\mathbf{x} - \mathbf{x}^J, h^J) \mathbf{p}_1(\mathbf{x}^J)$, $\mathbf{b}_2(\mathbf{x}) = w(\mathbf{x} - \mathbf{x}^J, h^J) \mathbf{p}_2(\mathbf{x}^J)$ and $\gamma_1(\mathbf{x}) = \mathbf{A}(\mathbf{x})^{-1} \mathbf{p}_1(\mathbf{x})$, the x'_i -derivative of the field function is written as

$$\begin{aligned}
& \frac{\partial u}{\partial x'_i} \simeq \frac{\partial u_h}{\partial x'_i} \\
& = \sum_{J \in \Lambda_1(x)} \left\{ \frac{\partial}{\partial x'_i} \gamma_1^\top(\mathbf{x}) \mathbf{b}_1(\mathbf{x}) + \gamma_1^\top(\mathbf{x}) \frac{\partial}{\partial x'_i} \mathbf{b}_1(\mathbf{x}) \right\} u^J \\
& + \sum_{J \in \Lambda_2(x)} \left\{ \frac{\partial}{\partial x'_i} \gamma_1^\top(\mathbf{x}) \mathbf{b}_2(\mathbf{x}) + \gamma_1^\top(\mathbf{x}) \frac{\partial}{\partial x'_i} \mathbf{b}_2(\mathbf{x}) \right\} u^J \\
& = \sum_{J \in \Lambda(x)} \frac{\partial \phi^J}{\partial x'_i} u^J
\end{aligned} \tag{14}$$

and thus the x_i -derivative can be obtained by the two-dimensional transformation of coordinates as

$$\begin{pmatrix} \frac{\partial \phi^J}{\partial x_1} \\ \frac{\partial \phi^J}{\partial x_2} \end{pmatrix} = \begin{pmatrix} c_1 & -c_2 \\ c_2 & c_1 \end{pmatrix} \begin{pmatrix} \frac{\partial \phi^J}{\partial x'_1} \\ \frac{\partial \phi^J}{\partial x'_2} \end{pmatrix} \quad (15)$$

3.3 Comparison of MLS approximation with conventional SPH approximation

The above MLS approximations and the SPH approximation are compared to investigate the reproducibility of a function with discontinuous derivative at a point $x_1 = 0.5$.

$$u(\mathbf{x}) = \begin{cases} (x_1 - 0.2)^2 & (x_1 \leq 0.5) \\ -(x_1 - 0.2)^2 + 0.18 & (0.5 < x_1) \end{cases} \quad (16)$$

The standard SPH approximation is written as follows:

$$u(\mathbf{x}) \simeq u_h(\mathbf{x}) = \sum_{J \in \Lambda(\mathbf{x})} \left(\frac{m^J}{\rho} \right) W(\mathbf{x} - \mathbf{x}^J, h) u^J \quad (17)$$

$$\frac{\partial u}{\partial x_i} \simeq \frac{\partial u_h}{\partial x_i} = \sum_{J \in \Lambda(\mathbf{x})} \left(\frac{m^J}{\rho} \right) \frac{\partial}{\partial x_i} W(\mathbf{x} - \mathbf{x}^J, h) u^J \quad (18)$$

where m is the mass, ρ is the density, $W(\mathbf{x}, h)$ is the smoothing function. In this study, the two-dimensional smoothing function with the cubic spline weight function $w(\mathbf{x}, h)$ as written in Eq. (4) is employed (see Liu and Liu 2003)

$$W(\mathbf{x}, h) = \frac{15}{7\pi h^2} w(\mathbf{x}, h) \quad (19)$$

Uniform nodal distribution ($\Delta x_1 = \Delta x_2 = 0.1$) is used (see Fig. 2). The smoothing lengths are set to $h^I = 1.2\Delta x_1$ ($I = 1, 2, \dots, 100$). Fig. 3 shows the conventional MLS shape function while Fig. 4 shows the MLS shape function with DBF. These shape functions are defined at the node \mathbf{x}^{45} where the Cartesian coordinates are expressed as $(x_1, x_2) = (0.45, 0.45)$. Comparing with the conventional MLS method, it is shown that the MLS shape function with DBF has the derivative discontinuity on the straight line $x_1 = 0.5$.

The approximate values of the function u at the positions of 10 nodes on a line $x_1 = 0.45$ are shown in Fig. 5 (a) with the exact values, while the approximate values of the x_1 -derivative $\partial u / \partial x_1$ are shown in Fig. 5 (b). The conventional SPH approximation gives poor accuracy due to the truncation of the smoothing function by the boundary as mentioned in the textbook by Liu and Liu (2003). Both results of the conventional SPH and the conventional MLS yield excessively smooth approximation near the discontinuous derivative line $x_1 = 0.5$. On the other hand, the MLS approximation with DBF agrees with the exact solution very well for both of the function u and its x_1 -derivative $\partial u / \partial x_1$.

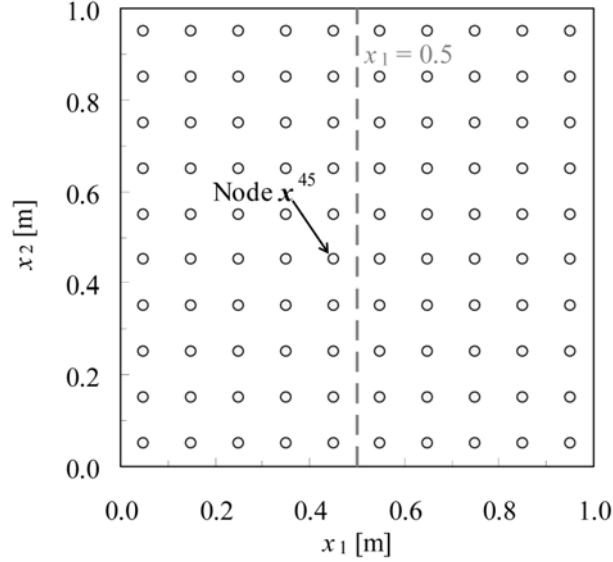


Fig. 2 Distribution of nodes \mathbf{x}^I ($I = 1, 2, \dots, 100$) and derivative discontinuous line

4. MLS-SPH (Moving Least Squares-Smoothed Particle Hydrodynamics)

4.1 MLS-SPH formulations

When the MLS approximate equation is substituted for the governing equations in Eqs. (1a-d), the following discretized equations at particles \mathbf{x}^I ($I = 1, 2, \dots, N$) are obtained.

Continuity equation:

$$\frac{d\rho^I}{dt} = -\rho^I \sum_{J \in \Lambda^I} \nabla^I \phi^J(\mathbf{x}^I) \cdot \mathbf{v}^J \quad (20a)$$

Equations of motion:

$$\frac{d\mathbf{v}^I}{dt} = -\frac{1}{\rho^I} \sum_{J \in \Lambda^I} \nabla^I \phi^J(\mathbf{x}^I) (p^J + q^{IJ}) \quad (20b)$$

Energy equation:

$$\frac{de^I}{dt} = -\frac{1}{\rho^I} \sum_{J \in \Lambda^I} (p^J + q^{IJ}) \nabla^I \phi^J(\mathbf{x}^I) \cdot \mathbf{v}^J \quad (20c)$$

Equation of state:

$$p^I = p(\rho^I, e^I) \quad (20d)$$

where Λ^I is the support domain of the particle. In addition, q^{IJ} corresponds to the Monaghan type artificial viscosity in the SPH paper by Monaghan (1992),

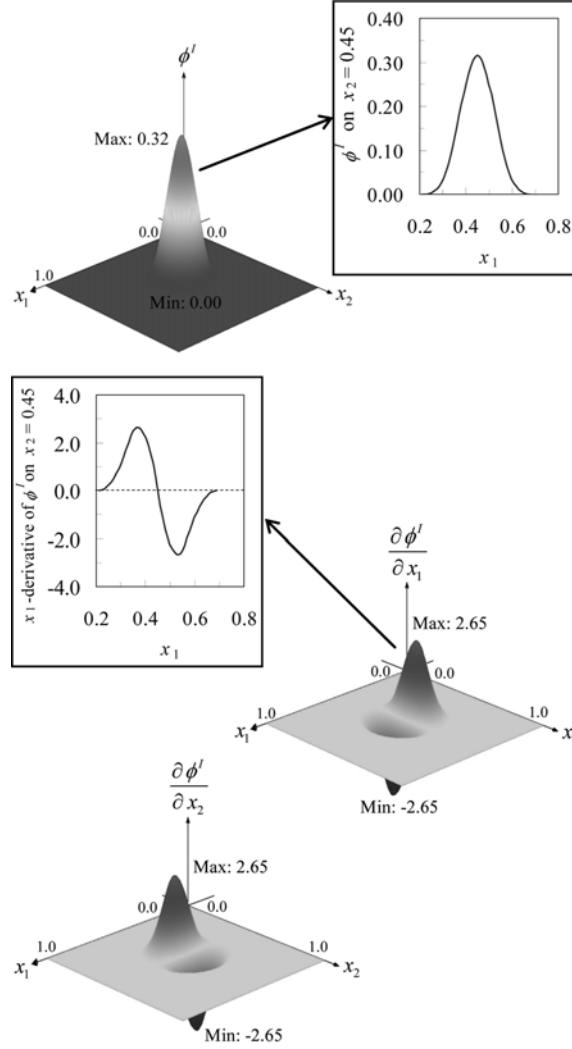


Fig. 3 Two-dimensional conventional MLS Shape function and the derivative at \mathbf{x}^I ($I = 45$)

$$q^{IJ} = \begin{cases} \bar{\rho}^{IJ} (\alpha_q \bar{c}_s^{-IJ} |\psi^{IJ}| + \beta_q |\psi^{IJ}|^2) & (\mathbf{v}^{IJ} \cdot \mathbf{x}^{IJ} < 0) \\ 0 & (\mathbf{v}^{IJ} \cdot \mathbf{x}^{IJ} \geq 0) \end{cases} \quad (21a)$$

$$\psi^{IJ} = \frac{\bar{h}^{IJ} \mathbf{v}^{IJ} \cdot \mathbf{x}^{IJ}}{|\psi^{IJ}|^2 + \psi^2} \quad (21b)$$

where c_s is the sound speed, α_q and β_q are parameters, ψ^{IJ} / \bar{h}^{IJ} means the divergence of the

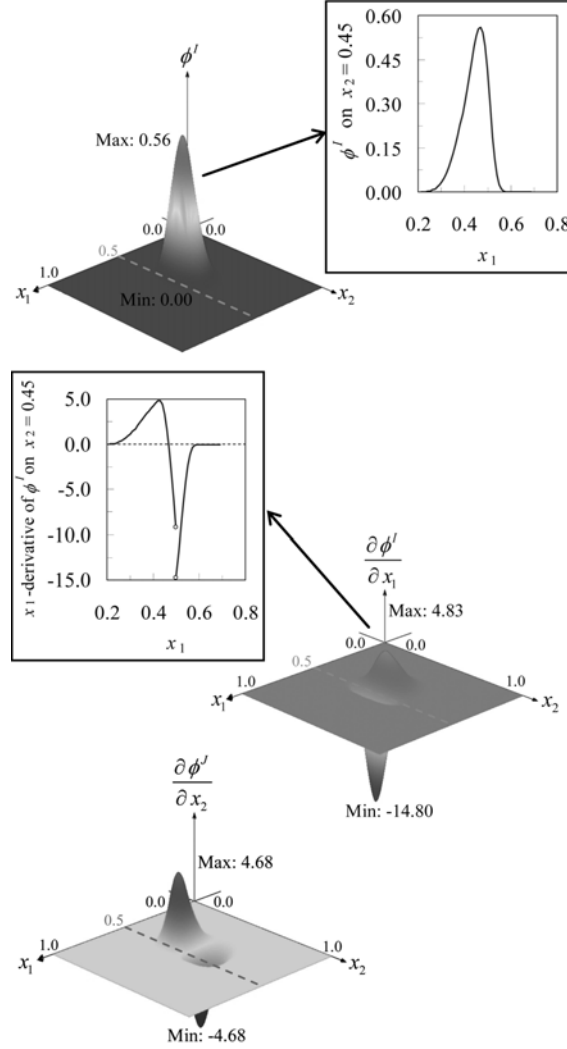


Fig. 4 Two-dimensional MLS Shape function with DBF and the derivative at \mathbf{x}^I ($I = 45$)

velocity between two particles, $\mathbf{v}^{IJ} \equiv \mathbf{v}^I - \mathbf{v}^J$, $\mathbf{x}^{IJ} \equiv \mathbf{x}^I - \mathbf{x}^J$, $\bar{c}_s^{IJ} \equiv (c_s^I + c_s^J)/2$, $\bar{\rho}^{IJ} \equiv (\rho^I + \rho^J)/2$, $\bar{h}^{IJ} \equiv (h^I + h^J)/2$ and $\psi = 0.1h^{IJ}$.

4.2 Time marching

In this study, the leapfrog method is implemented because its efficiency is reasonable with respect to accuracy and memory capacity in the time integration. At the first step the following equations at particles \mathbf{x}^I ($I = 1, 2, \dots, N$) are computed.

Update of density:

$${}^{1/2}\rho^I = {}^0\rho^I + \frac{\Delta t}{2} \left(\frac{d\rho^I}{dt} \right) \quad (22a)$$

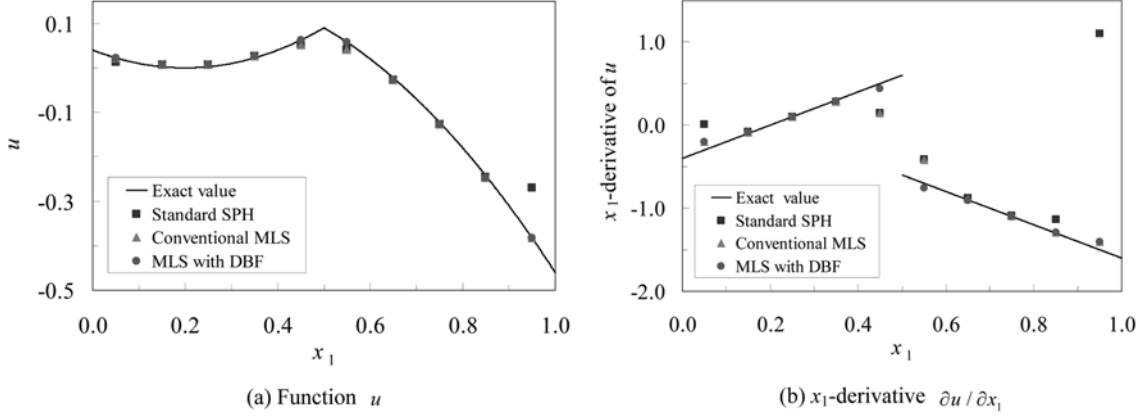


Fig. 5 SPH approximation and MLS approximations of function and the derivative

Update of velocity:

$${}^{1/2}\mathbf{v}^I = {}^0\mathbf{v}^I + \frac{\Delta t}{2} \left(\frac{d\mathbf{v}^I}{dt} \right) \quad (22b)$$

Update of specific internal energy:

$${}^{1/2}e^I = {}^0e^I + \frac{\Delta t}{2} \left(\frac{de^I}{dt} \right) \quad (22c)$$

Update of particle position:

$${}^{1/2}\mathbf{v}_h({}^0\mathbf{x}^I) = \sum_{J \in \Lambda^I} \phi^J({}^0\mathbf{x}^I) {}^{1/2}\mathbf{v}^J \quad (22d)$$

$${}^1\mathbf{x}^I = {}^0\mathbf{x}^I + \Delta t {}^{1/2}\mathbf{v}_h({}^0\mathbf{x}^I) \quad (22e)$$

where Δt is the time increment. At the n -th step the following equations at particles \mathbf{x}^I ($I = 1, 2, \dots, N$) are computed and approximate solutions at each time step are obtained.

Update of density:

$${}^{n+\frac{1}{2}}\rho^I = {}^{n-\frac{1}{2}}\rho^I + \Delta t \left(\frac{d\rho^I}{dt} \right) \quad (23a)$$

Update of velocity:

$${}^{n+\frac{1}{2}}\mathbf{v}^I = {}^{n-\frac{1}{2}}\mathbf{v}^I + \Delta t \left(\frac{d\mathbf{v}^I}{dt} \right) \quad (23b)$$

Update of specific internal energy:

$${}^{n+\frac{1}{2}}e^I = {}^{n-\frac{1}{2}}e^I + \Delta t \left(\frac{de^I}{dt} \right) \quad (23c)$$

Update of particle position:

$${}^{n+\frac{1}{2}}\mathbf{v}_h({}^n\mathbf{x}^I) = \sum_{J \in \Lambda^I} \phi^J({}^n\mathbf{x}^I) {}^{n+\frac{1}{2}}\mathbf{v}^J \quad (23d)$$

$${}^{n+1}\mathbf{x}^I = {}^n\mathbf{x}^I + \Delta t {}^{n+\frac{1}{2}}\mathbf{v}_h({}^n\mathbf{x}^I) \quad (23e)$$

5. Shock-tube problems (Contact discontinuity face of gas)

Shock-tube problems of ideal gas (air) with analysis domain $-0.5\text{ m} \leq x_1 \leq 0.5\text{ m}$ as shown in Fig. 6 are handled in order to investigate the effectiveness of the MLS-SPH method with DBF for the contact discontinuity face. The equation of state for ideal gas is expressed as follows:

$$p = (\gamma - 1)\rho e \quad (24)$$

where γ is the specific ratio and the value for air is 1.4. An exact solution obtained with the exact Riemann solver by Toro (1997) is available for comparison. In this analysis, Case 1 (the density ratio is 1 to 0.25 and the pressure ratio is 1 to 0.179) and Case 2 (the density ratio is 1 to 0.125 and the pressure ratio is 1 to 0.1) are computed. In other words, the different density and pressure ratios are used in Case 1 and Case 2. Case 1 has been solved by several SPH researchers such as Hernquist and Katz (1989), Liu *et al.* (2003), Hongbin and Xin (2005) and Sigalotti *et al.* (2006) for verification of the method. On the other hand, Case 2 was initially solved by Sod (1978) and is rarely solved by particle methods because of a more severe initial condition than Case 1. The total

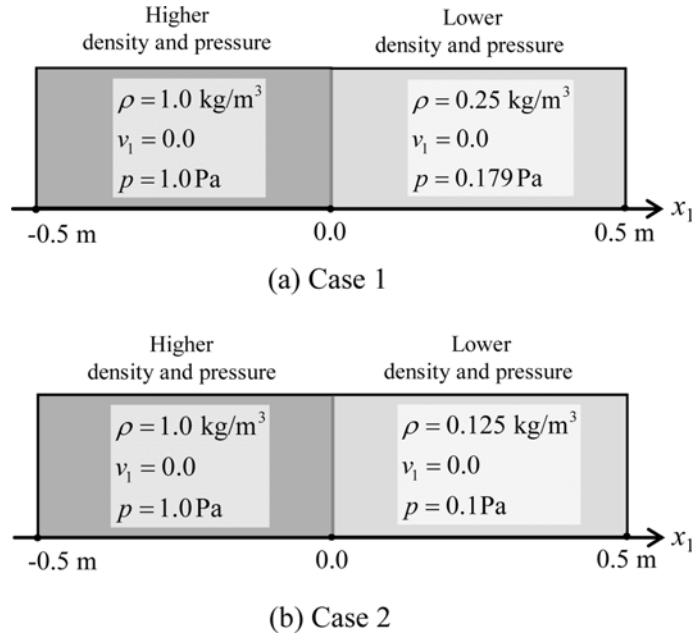


Fig. 6 Analysis models of shock-tube problem

number of particles is 400×9 and the initial particle spacing is set to $\Delta x_1 = \Delta x_2 = 1.0/400\text{m}$. The time increment Δt and the smoothing lengths h^I ($I=1, 2, \dots, 3600$) are constant throughout the computation, and they are set to $\Delta t = 1.0 \times 10^{-4}\text{s}$ (Case 1) and $\Delta t = 5.0 \times 10^{-5}\text{s}$ (Case 2) and $h^I = 2\Delta x_1$ ($I=1, 2, \dots, N$) respectively. The artificial viscosity parameters are set as $\alpha_q = 1.0$ and $\beta_q = 1.0$. In this analysis, three different computational methods, i.e., the standard SPH method, the conventional MLS-SPH method and the MLS-SPH method with DBF are compared. The standard SPH formulation has symmetric property and has been utilized by Monaghan (1994), Morris and Monaghan (1997), Liu *et al.* (2003), etc. The discontinuous derivative face as shown in Fig. 1 (b) is assumed to be located in the middle of the edge particles with higher density and those with lower density.

Fig. 7 shows the density distributions, the velocity distributions, and the pressure distributions at $t=0.2\text{s}$ in Case 1. In the standard SPH method and the conventional MLS-SPH method, large numerical oscillation arises in the domain near the contact discontinuity face. In the MLS-SPH method with DBF, it is possible to suppress this numeric oscillation. Fig. 8 shows the particle distributions in the interval $0.1\text{m} \leq x_1 \leq 0.35\text{m}$ in the MLS-SPH method with DBF. It can be confirmed that the particle distributions at $t=0.2\text{s}$ becomes dense in the compression part of gas

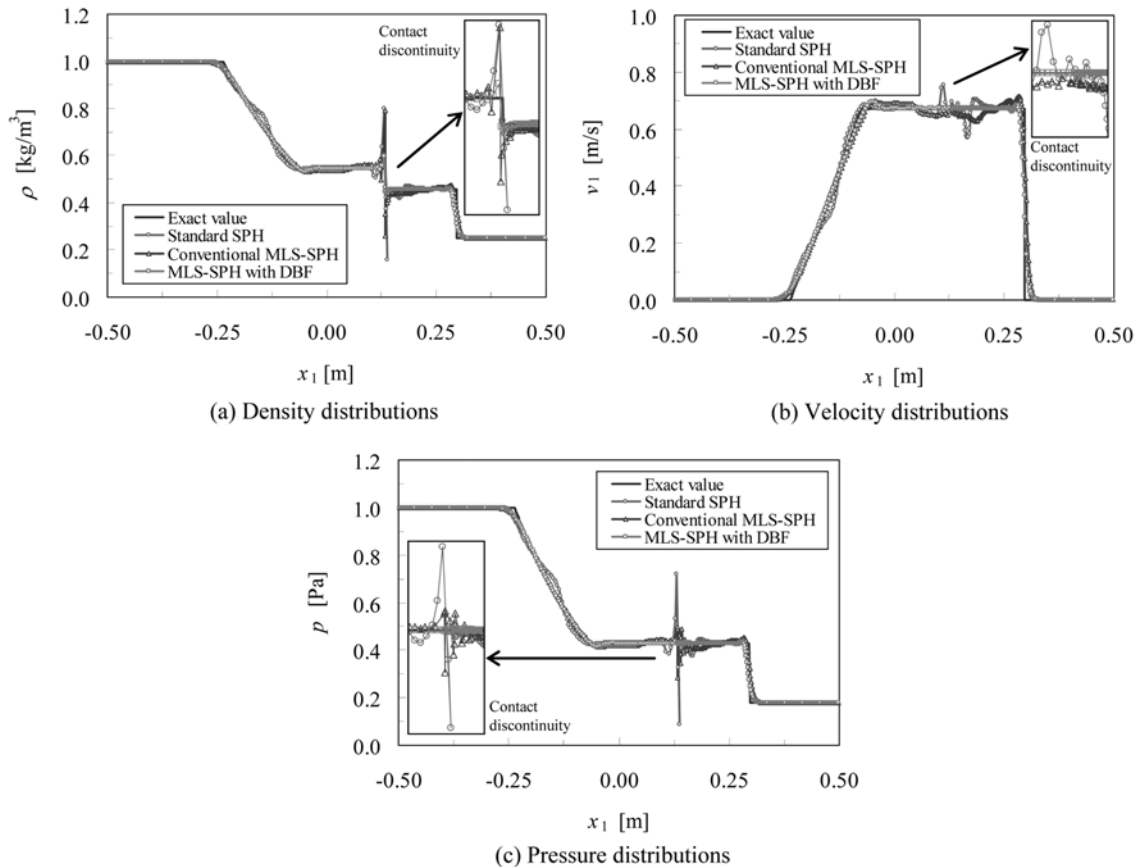


Fig. 7 Density, velocity and pressure distributions at $t=0.2\text{s}$ in Case 1

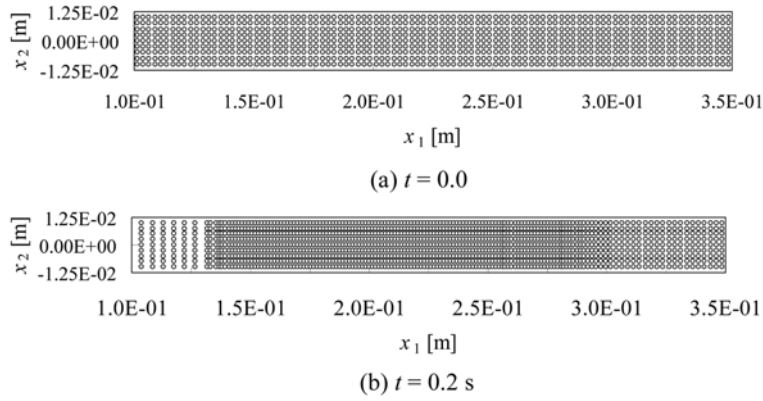


Fig. 8 Particle distributions in Case 1 (MLS-SPH with DBF)

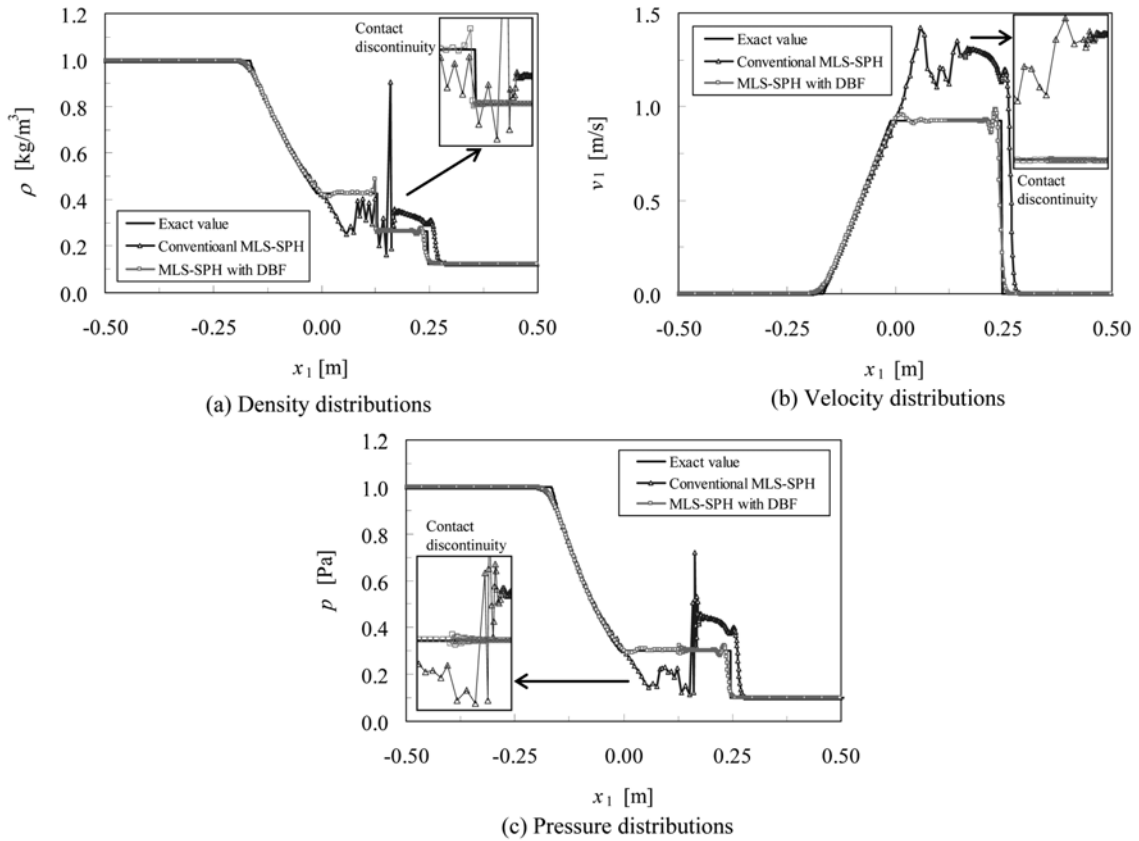


Fig. 9 Density, velocity and pressure distributions at $t = 0.14s$ in Case 2

and sparse in the expansion part of gas. Fig. 9 shows the density distributions, the velocity distributions, and the pressure distributions at $t = 0.14s$ in Case 2. Only the results of the conventional MLS-SPH method and the MLS-SPH method with DBF are compared because the

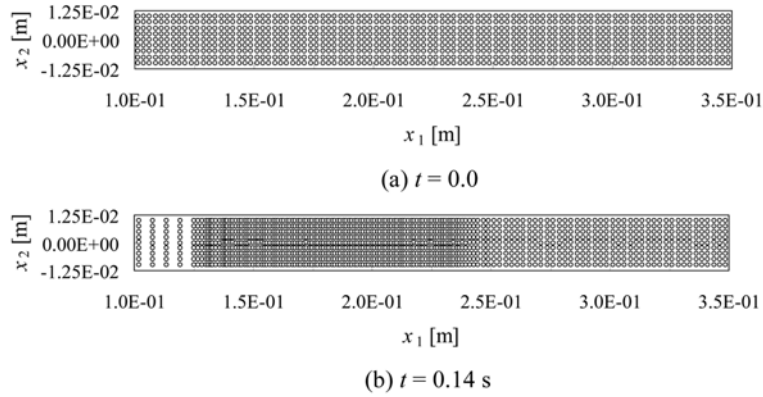


Fig. 10 Particle distributions in Case 2 (MLS-SPH with DBF)

computation using the standard SPH method breaks down due to an enormous amplitude of numerical oscillation. The MLS-SPH method with DBF can reasonably suppress the numerical oscillation as well as in Case 1. Fig. 10 shows the particle distributions in the interval $0.1 \text{ m} \leq x_1 \leq 0.35 \text{ m}$ in the MLS-SPH method with DBF. The particle distributions at $t = 0.14 \text{ s}$ form sparse and dense domains in the expansion and compression part of gas respectively as well as in Case 1.

6. UNDEX problems (Gas-liquid interface)

UNDEX problems are analyzed in order to investigate the effectiveness of the MLS-SPH method with DBF for discontinuous derivative on the gas-liquid interface. On the gas-liquid interface, it is necessary to satisfy kinematical and dynamic conditions on the assumption of inviscid flow as shown in Eq. (25).

Kinematical condition:

$$\mathbf{n} \cdot \mathbf{v}_{\text{gas}} = \mathbf{n} \cdot \mathbf{v}_{\text{liquid}} \quad (25a)$$

Dynamic condition (or traction equilibrium):

$$p_{\text{gas}} = p_{\text{liquid}} \quad (25b)$$

where \mathbf{n} is the unit vector normal to the gas-liquid interface. Because the normal component of velocity is much larger than the tangent component near the gas-liquid interface, the velocity and the pressure is assumed to be continuous in this study. However, the gradients of velocity and pressure are discontinuous naturally. It is, therefore, effective to apply the MLS approximation with DBF to the gradients of velocity and pressure in the governing equations.

In this analysis, an artificial high explosive detonation model in Liu and Liu (2003) is adopted. In this model, the detonation process is not directly considered and it is assumed that the gas begins to expand when the computation starts. The initial difference of pressure at the interface between the explosive gas and water is in the order of 10^9 Pa .

The Jones-Wilkins-Lee (JWL) equation is used as the equation of state for explosive gas of TNT.

$$p = A \left(1 - \frac{\omega \eta}{R_1}\right) \exp\left(-\frac{R_1}{\eta}\right) + B \left(1 - \frac{\omega \eta}{R_2}\right) \exp\left(-\frac{R_2}{\eta}\right) + \omega \eta^0 \rho e \quad (26)$$

where η is the ratio of current density to initial density and it is defined as

$$\eta = \frac{\rho}{\rho_0} \quad (27)$$

The parameters in Eq. (26) are shown in Table 1. The following equation is also utilized as the equation of state for water.

$$p = \begin{cases} \alpha_1 \mu + \alpha_2 \mu^2 + \alpha_3 \mu^2 + (b_0 + b_1 \mu + b_1 \mu^2)^0 \rho e & (\mu \geq 0) \\ \alpha_1 \mu + (b_0 + b_1 \mu)^0 \rho e & (\mu < 0) \end{cases} \quad (28)$$

where μ is the ratio of current density variation to initial density and it is defined as

$$\mu = \frac{\rho}{\rho_0} - 1 \quad (29)$$

Eq. (28) is applicable for $\eta = 0.8$ and the parameters are shown in Table 2.

The time increment Δt is determined as the following equation with the Courant number C .

$$\Delta t = \min_{1 \leq I \leq N} \frac{C h^I}{v_i^I} \quad (30a)$$

$$v_i^I = h^I (\nabla \cdot \mathbf{v})^I + c_s^I + 1.2 (\alpha_q c_s^I + \beta_q h^I |(\nabla \cdot \mathbf{v})^I|) \quad (30b)$$

where N is the total number of particles and $(\nabla \cdot \mathbf{v})^I$ is defined as

$$(\nabla \cdot \mathbf{v})^I = \sum_{J \in \Lambda^I} \nabla \phi^J(\mathbf{x}^I) \cdot \mathbf{v}^J \quad (31)$$

In this study, the Courant number is $C = 0.3$. The artificial viscosity parameters are set to $\alpha_q = 1.0$ and $\beta_q = 10.0$.

Table 1 Parameters of equation of state for explosive gas (TNT)

Symbol	Meaning	Value
A	Fitting coefficient	3.712×10^{11} Pa
B	Fitting coefficient	3.21×10^9 Pa
R_1	Fitting coefficient	4.15
R_2	Fitting coefficient	0.95
ω	Fitting coefficient	0.30
ρ_0	Initial density	1.63×10^3 kg/m ³

Table 2 Parameters of equation of state for water ($\mu < 0.8$)

Symbol	Meaning	Value
α_1	Fitting coefficient	2.19×10^9 Pa
α_2	Fitting coefficient	9.224×10^9 Pa
α_3	Fitting coefficient	8.767×10^9 Pa
b_0	Fitting coefficient	0.4934
b_1	Fitting coefficient	1.3937
${}^0\rho$	Initial density	1.0×10^3 kg/m ³

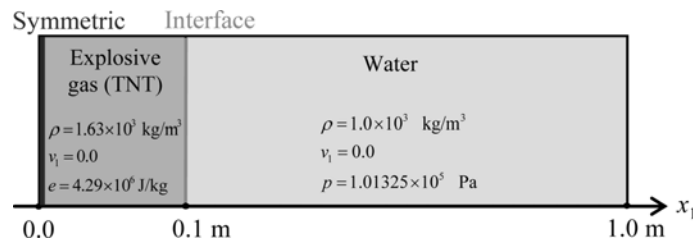


Fig. 11 Analysis model of underwater explosion of a TNT slab charge

6.1 UNDEX of a TNT slab charge

The analysis model of UNDEX of a TNT slab charge is shown in Fig. 11. The analysis domain is defined as the interval of $0.0 \leq x_1 \leq 1.0$ m with symmetric boundary at $x_1 = 0.0$. A similar problem using the same TNT slab, with a larger analysis domain of interval $0.0 \leq x_1 \leq 1.0$ m, was solved in order to compare the pressure peak at different locations of the real and artificial detonation models given in Liu and Liu (2003). In this study, the full interval of $-1.0 \text{ m} \leq x_1 \leq 1.0 \text{ m}$ is modeled in order to avoid the treatment of symmetrical boundary condition. The total number of particles is 1000×9 and the minimum distance between neighboring particles is $\Delta x_1 = \Delta x_2 = .10 / 500 \text{ m}$. The smoothing lengths are constant and set to $h^f = 2\Delta x_1$ in this analysis. Three different computational methods, i.e., the standard SPH method, the conventional MLS-SPH method and the MLS-SPH method with DBF are compared. In the MLS-SPH method with DBF, x_d^f on the gas and liquid interface is defined as the midpoint between gas and liquid particles.

Fig. 12 shows the density distributions, the velocity distributions, and the pressure distributions at $t = 1.2 \times 10^{-4}$ and the gas-liquid interface exists at $x_1 = 0.201 \text{ m}$. The numerical pressure oscillation arises at the gas-liquid interface in the result of the standard SPH method and the conventional MLS-SPH method. Comparing the conventional MLS-SPH with the SPH, the conventional MLS-SPH gives even worse results regarding the density and velocity. This results from averaging or smoothing the physical quantities of particles on both sides of the interface in the SPH formulation. On the other hand, the MLS-SPH method with DBF is able to remarkably suppress the pressure oscillation caused by the interface as shown in Fig. 12 (c). However, slight numerical oscillation near the underwater shock wave arises because the pressure discontinuity is not considered there. It is necessary to investigate the use of a jump function for the shock wave in order to analyze problems with a large pressure difference between the front and the rear of shock wave more accurately. Fig. 13 shows particle distribution in the interval $1.0 \text{ m} \leq x_1 \leq 1.6 \text{ m}$ in the MLS-SPH

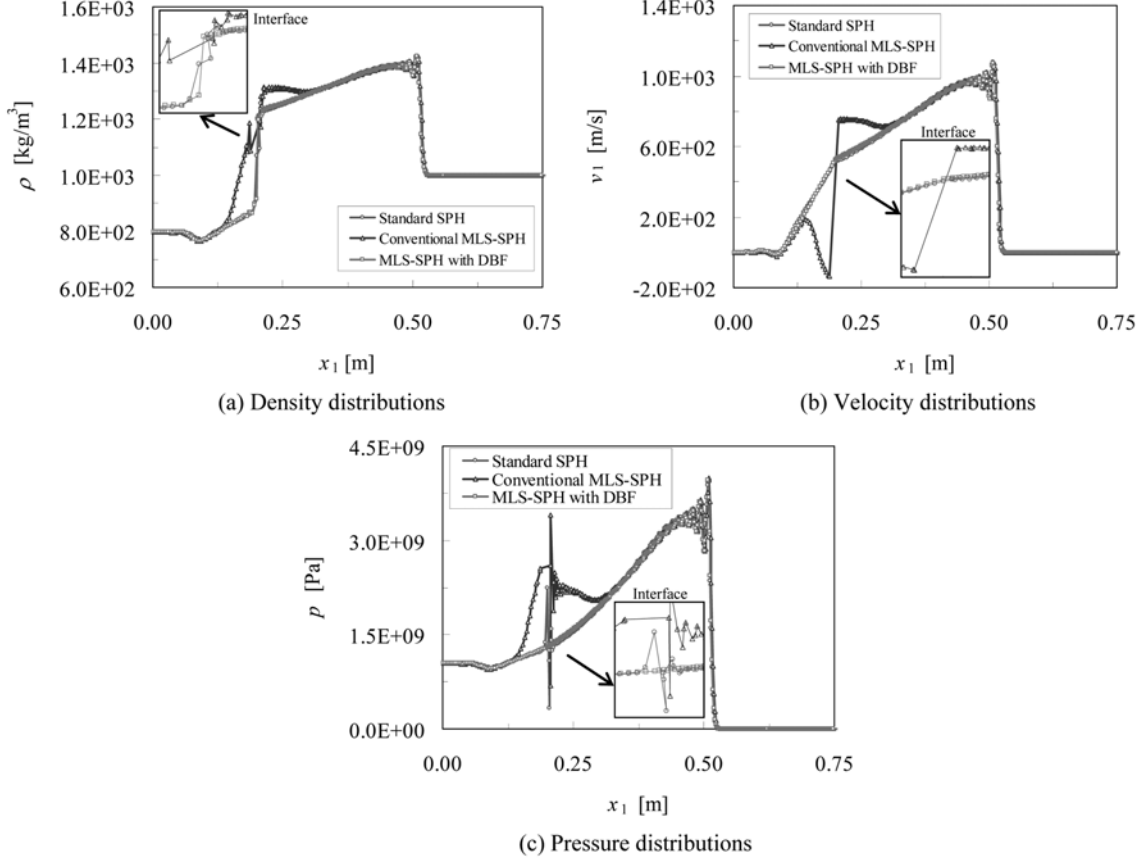


Fig. 12 Density, velocity and pressure distributions at $t = 1.2 \times 10^{-4}$ s

method with DBF. The particle distributions at $t = 1.2 \times 10^{-4}$ form sparse and dense domains in the gas expansion and water compression part of gas respectively.

6.2 UNDEX of a square TNT charge

Fig. 14 shows an analysis model of UNDEX of a square TNT charge in a rigid container. The effectiveness is verified in the two-dimensional problem. Fig. 15 shows liquid particles and virtual fixed particles arranged near the rigid wall. When a liquid particle \mathbf{x}^I approaches this virtual particle \mathbf{x}^J , the repulsive force \mathbf{f}_r^I is exerted on the liquid particle to prevent the liquid particle from penetrating the rigid wall. The repulsive force \mathbf{f}_r^I is the same as Liu *et al.* (2003) and defined as

$$\mathbf{f}_r^I = \begin{cases} v_a^2 \left\{ \left(\frac{r_w}{r^{IJ}} \right)^{12} - \left(\frac{r_w}{r^{IJ}} \right)^6 \right\} \frac{\mathbf{x}^I - \mathbf{x}^J}{(r^{IJ})^2} & (r^{IJ} \geq r_w) \\ 0 & (r^{IJ} < r_w) \end{cases} \quad (32)$$

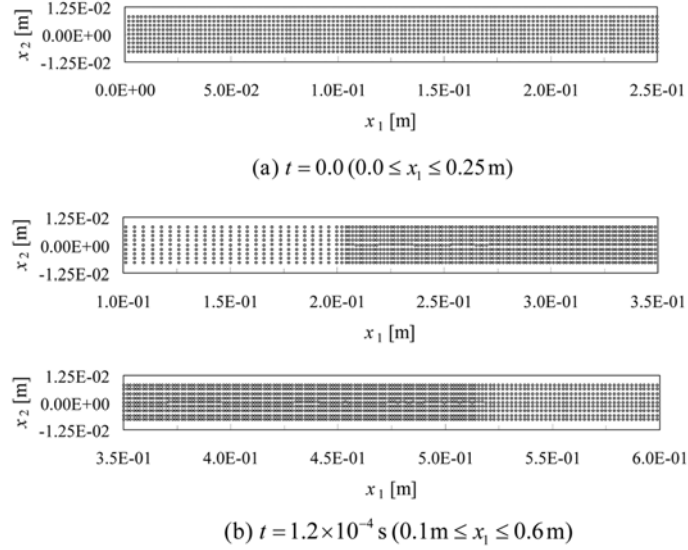


Fig. 13 Particle distributions (MLS-SPH with DBF)

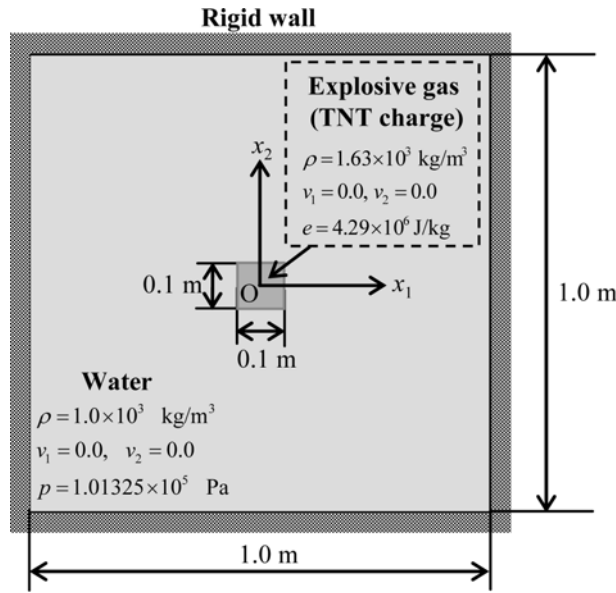


Fig. 14 Analysis model of underwater explosion problem of a square TNT charge

where $r^{IJ} = |\mathbf{x}^I - \mathbf{x}^J|$, $r_w = 0.5\Delta x_1$, and v_a is the average of the absolute value of velocities expressed as

$$v_a = \frac{\sum_{I=1}^N |v^I|}{N} \quad (33)$$

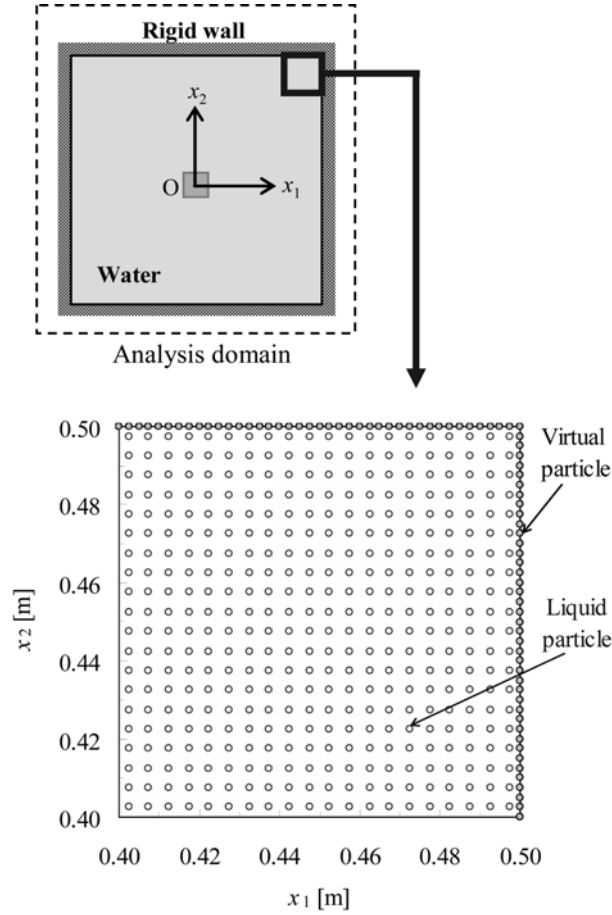


Fig. 15 Particle distribution near rigid wall

where N is the total number of the gas particles, the liquid particles and the virtual particles. Fig. 16 also shows gas particles, liquid particles and interface nodes \mathbf{x}_c^I ($I = 1, 2, \dots, N_c$) located near the gas-liquid interface. The interface node has connectivity between other nodes and represents the geometry of the gas-liquid interface. When the DBF is applied to the domain near the gas-liquid interface, it is necessary to find a point \mathbf{x}_d^J and a normal vector \mathbf{c}^J for a particle \mathbf{x}^J . In this paper, the interface node \mathbf{x}_c^I that is the nearest from a particle \mathbf{x}^J is regarded as \mathbf{x}_d^J . The positions of the interface nodes are updated in according to the following equation.

$${}^{n+\frac{1}{2}}\mathbf{v}_h({}^n\mathbf{x}_c^I) = \sum_{J \in \Lambda_c^I} \phi^J({}^n\mathbf{x}_c^I) {}^{n+\frac{1}{2}}\mathbf{v}^J \quad (34a)$$

$${}^{n+1}\mathbf{x}_c^I = {}^n\mathbf{x}_c^I + \Delta t {}^{n+\frac{1}{2}}\mathbf{v}_h({}^n\mathbf{x}_c^I) \quad (34b)$$

where Λ_c^I is the support domain at the interface node \mathbf{x}_c^I . The unit normal vector \mathbf{n}_c^I at the interface

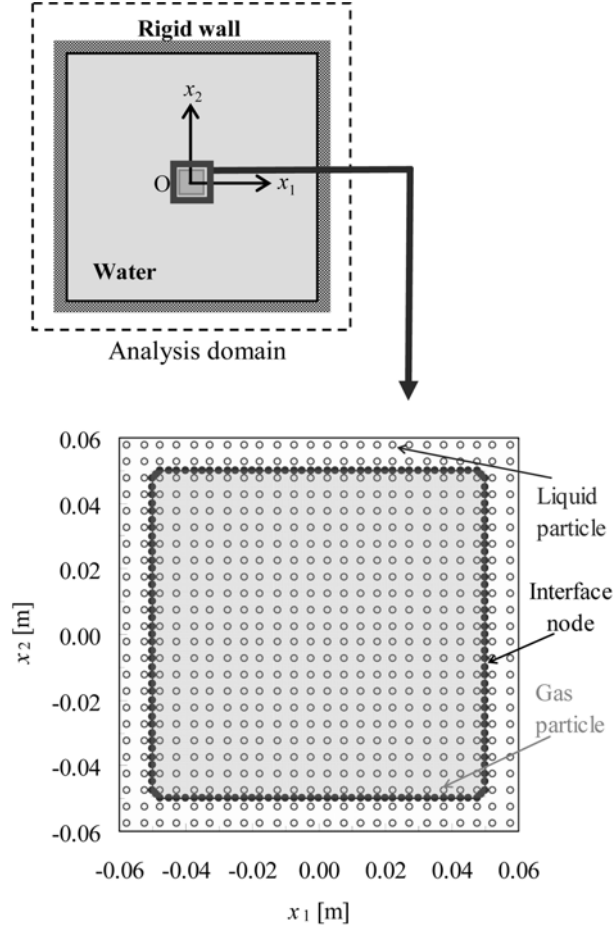


Fig. 16 Particle distribution near gas-liquid interface

node \mathbf{x}_c^I is obtained from weighted average (see Fig. 17).

$$\mathbf{n}_c^I = \frac{\mathbf{n}_1^I l_1^I + \mathbf{n}_2^I l_2^I}{|\mathbf{n}_1^I l_1^I + \mathbf{n}_2^I l_2^I|} \quad (35)$$

The unit normal vector \mathbf{c}^J is defined as

$$\mathbf{c}^J = \begin{cases} \mathbf{n}_I^c & (g(\mathbf{x}^J) \geq 0) \\ -\mathbf{n}_I^c & (g(\mathbf{x}^J) < 0) \end{cases} \quad (36)$$

where $g(\mathbf{x}^J) = \mathbf{n}_c^I \cdot (\mathbf{x}^J - \mathbf{x}_c^I)$.

The total number of internal particles is 200×200 , the total number of virtual particles 1600 and the total number of interface nodes is 160. The initial minimum distance between internal

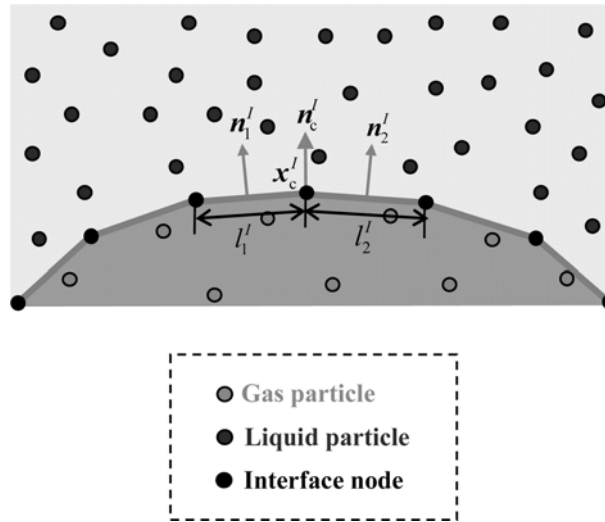


Fig. 17 Calculation of unit normal vector at an interface node x_c^I

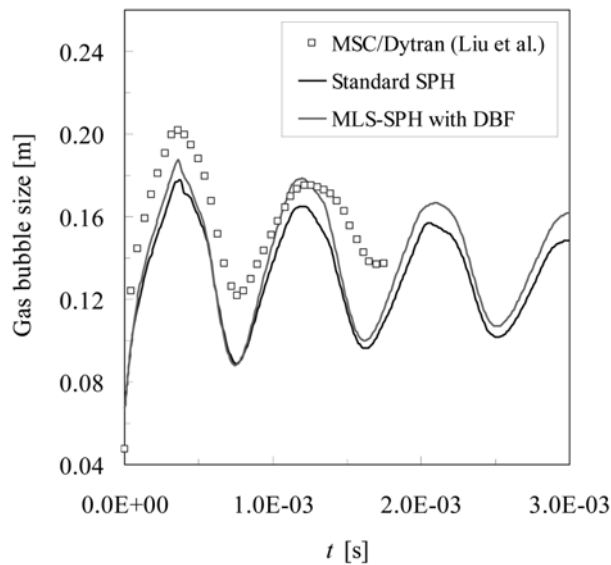


Fig. 18 Time histories of gas bubble size

neighboring particles is set to $\Delta x_1 = \Delta x_2 = 1.0/200\text{m}$. In this problem, as the density of the particle distribution changes largely, the smoothing length changes according to the equation by Benz (1989) at each time step. The Benz's equation defines the material time-derivative of the smoothing length as

$$\frac{d h^I}{dt} \simeq \frac{h^I}{D} (\nabla \cdot \mathbf{v})^I \quad (37)$$

where D is the dimension number and it is set up as $D = 2$ in this study. In this equation, the third

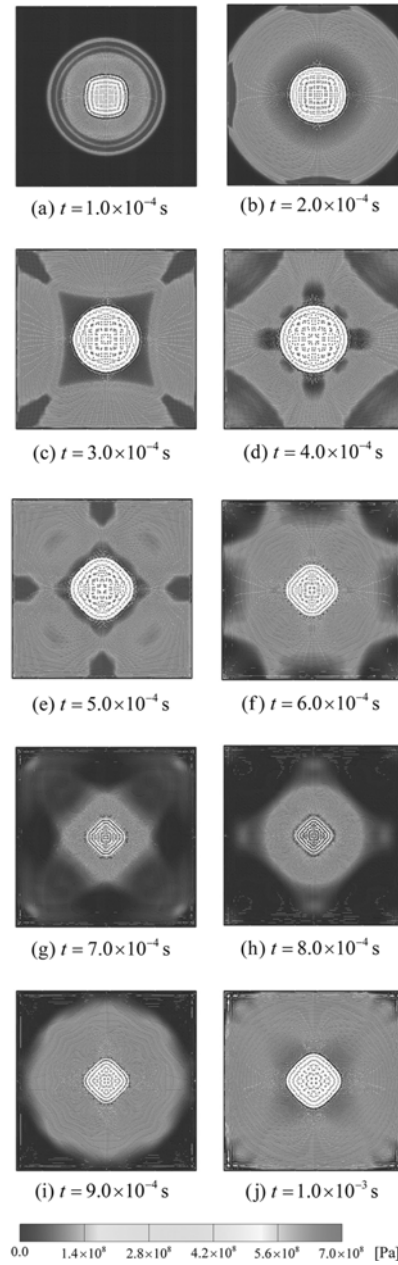


Fig. 19 Particle distributions and pressure distributions (standard SPH)

invariant of the deformation gradient \mathbf{F} is approximated by the ratio of the current smoothing length h to the initial smoothing length 0h .

$$\det \mathbf{F} \simeq \left(\frac{h}{{}^0h} \right)^D \quad (38)$$

The time marching of the smoothing length is based on the forward Euler scheme and written as

$${}^{n+1}h^I = {}^n h^I + \Delta t \left(\frac{d h^I}{dt} \right) \quad (39)$$

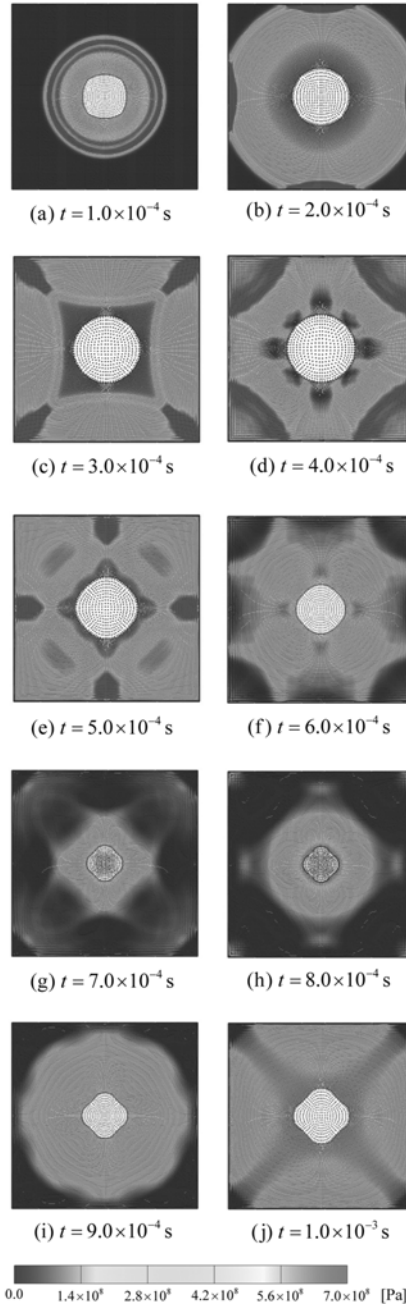


Fig. 20 Particle distributions and pressure distributions (MLS-SPH with DBF)

The initial smoothing lengths are set to ${}^0h^f = 2 \Delta x_1 = 2 \Delta x_2$. In this analysis, the standard SPH method and the MLS-SPH method with DBF are compared because the computation of conventional MLS-SPH method fails when an underwater shock wave reflects from the rigid wall.

Fig. 18 shows the time histories of bubble size with the approximate solutions of MSC/Dytran code in Liu, Liu, Lam and Zong (2003). The bubble size is the maximum value of the distances between the center of analysis domain and each gas particle. The MSC/Dytran is a grid-based code and the numerical solutions are obtained by the interpolation in cells. The gas bubble pulsation can be confirmed in Fig. 18. The results of the standard SPH and the MLS-SPH with DBF are close to that of the MSC/Dytran. Fig. 19 and 20 show the pressure distributions and the particle distributions at ten representative instants until $t = 1.0 \times 10^{-3}$ s in the underwater explosion process. The results of the standard SPH and the MLS-SPH with DBF are shown in Fig. 19 and Fig. 20 respectively. The interface nodes and the connectivity are also depicted to make the shape of the gas-liquid interface clear in Fig. 20. When the underwater shock wave propagates, the gas particles are distributed sparsely in the gas domain and the water particles become dense near the interface. As results, large inhomogeneity arises in the gas and liquid domains near the interface. The internal gas particles in the standard SPH is irregular, while those in the MLS-DBF is quite regular and stable

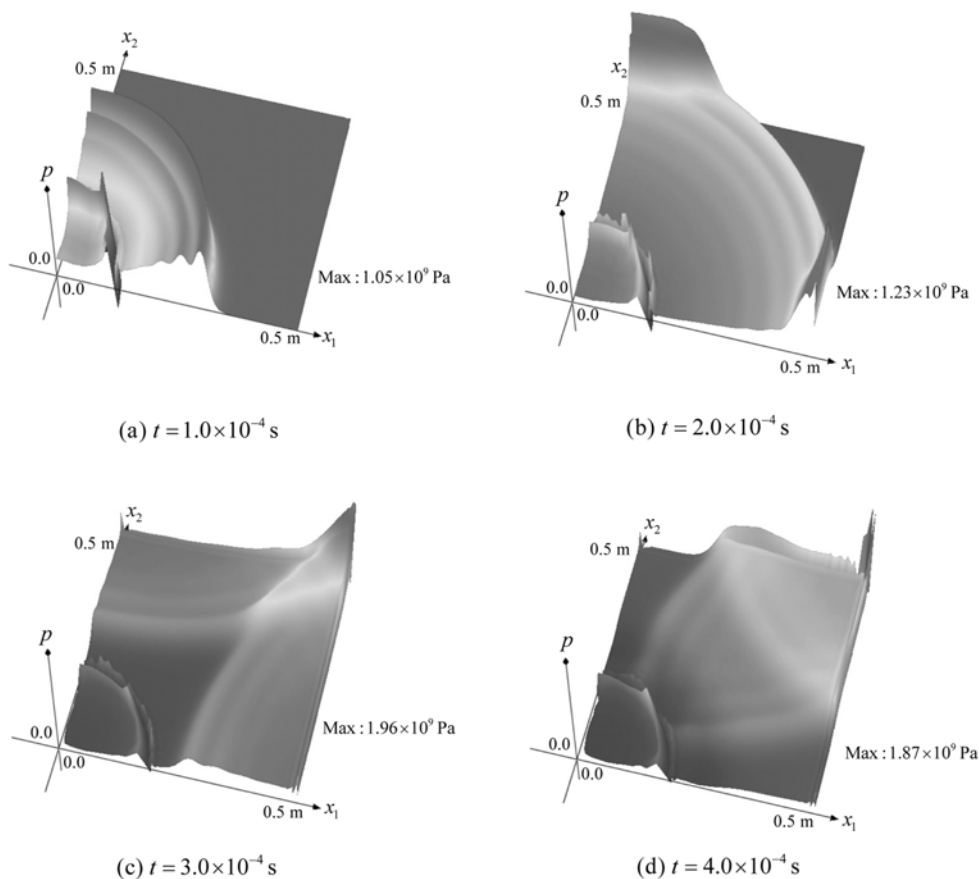


Fig. 21 Pressure distributions (standard SPH)

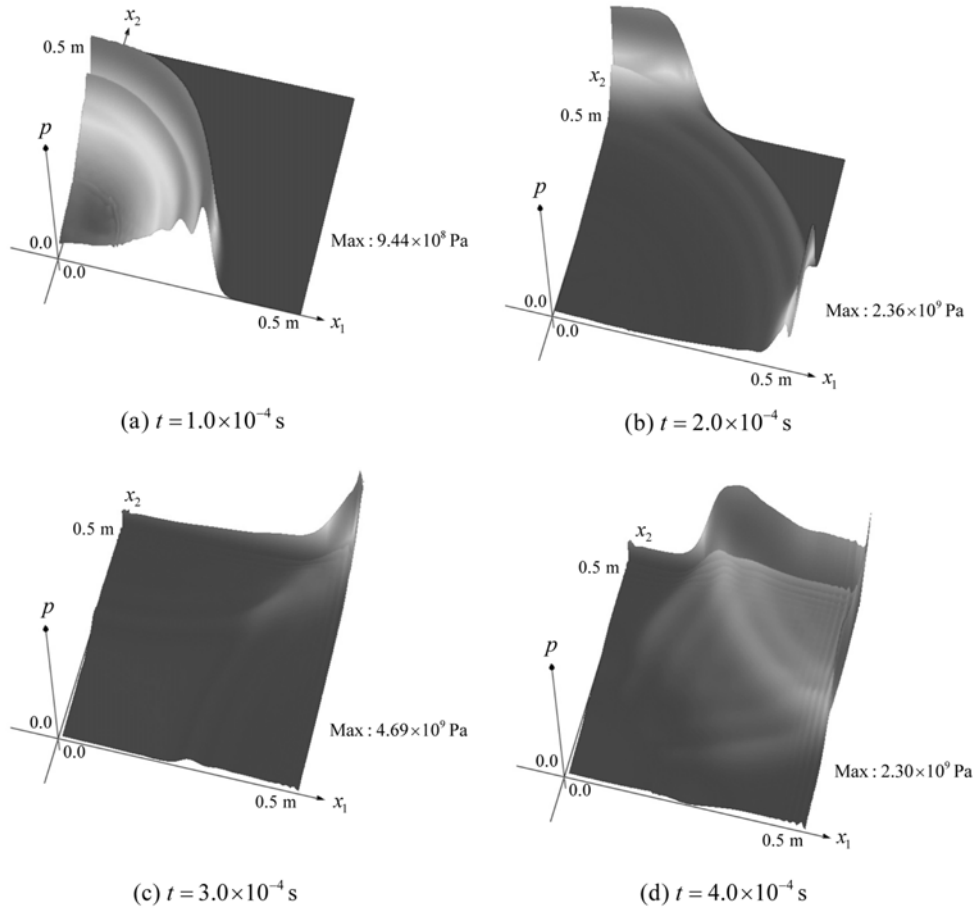


Fig. 22 Pressure distributions (MLS-SPH with DBF)

throughout the computation. The pressure oscillates near the interface in the standard SPH, while the pressure changes smoothly there in the MLS-SPH with DBF. The shock wave reaches the surrounding rigid wall at around the instant of $t = 2.0 \times 10^{-4}$ s. After the wave is reflected from the rigid wall, the explosive gas bubble repeats the expansion and contraction. Similar results can be found in Liu, Liu, Lam and Zong (2003). Figs 21 and 22 show the pressure distributions of the standard SPH and the MLS-SPH with DBF at four representative instants until $t = 4.0 \times 10^{-4}$ s respectively. The pressure oscillation with relative large peak arises near the interface in the standard SPH as shown in Fig. 21, where the nonphysical peak does not become small. On the other hand, such nonphysical pressure is not seen and the pressure distribution remains smooth in the MLS-SPH with DBF as shown in Fig. 22.

7. Conclusions

In the present study, UNDEX problems were analyzed using the MLS-SPH method with DBF for

the domain near to the gas-liquid interface in order to investigate discontinuous derivative on the interface. In the analysis using the MLS-SPH with DBF, the numerical oscillation of pressure that appeared in the standard SPH and the conventional MLS-SPH was suppressed sufficiently. The effectiveness of using the MLS-SPH with DBF method for solving UNDEX problems can be concluded because it was shown that solutions obtained when using the MLS-SPH with DBF method were more accurate and stable near the gas-liquid interface as compared to using the standard SPH or the conventional MLS-SPH. Extension to the three-dimensional analysis and application to triple solid-liquid-gas interaction problems are future works to be conducted.

Acknowledgement

This research was partially supported by Grant-in-Aid for Scientific Research (B) in 2005 and 2006, Ministry of Education, Culture, Sports, Science and Technology. The authors highly acknowledge this support.

References

- Belytschko, T., Lu, Y.Y. and Gu, L. (1994), "Element-free Galerkin methods", *Int. J. Numer. Methods. Eng.*, **37**, 229-256.
- Benz, W. (1989), "Smoothed particle hydrodynamics: a review", NATO Workshop, Les Arcs, France.
- Chen, J.K., Beraun, J.E. and Carney T.C. (1999), "A corrective smoothed particle method for boundary value problems in heat conduction", *Comput. Methods. Appl. Mech. Eng.*, **46**, 231-252.
- Dilts, G.A. (1999), "Moving-least-squares-particle hydrodynamics - I. consistency and stability", *Int. J. Numer. Methods. Eng.*, **44**, 1115-1155.
- Dilts, G.A. (2000), "Moving-least-squares-particle hydrodynamics-II. conservation and boundaries", *Int. J. Numer. Methods. Eng.*, **48**, 1503-1524.
- de Borst, R., Réthoré, J. and Abellan, M.A. (2008), "Two-scale approaches for fracture in fluid-saturated porous media", *Interaction and Multiscale Mechanics, An Int. J.*, **1**(1), 83-101.
- Gingold, R.A. and Monaghan, J.J. (1977), "Smoothed particle hydrodynamics: theory and application to non-spherical stars", *Monthly Notices of the Royal Astronomical Society*, **181**, 375-389.
- Hernquist, L. and Katz N. (1989), "TreeSPH - A unification of SPH with the hierarchical tree method", *The Astrophysical J. Supplement Series*, **70**, 419-446.
- Hongbin, J. and Xin, D. (2005), "On criterions for smoothed particle hydrodynamics kernels in stable field", *J. Comput. Phys.*, **202**, 699-709.
- Jahromi, H.Z., Izzuddin, B.A. and Zdravkovic, L. (2008), "Partitioned analysis of nonlinear soil-structure interaction using iterative coupling", *Interaction and Multiscale Mechanics, An Int. J.*, **1**(1), 33-51.
- Kobashi, W. and Matsuo, A. (2005), "Numerical study on underwater explosion simulation surrounded by an iron wall using smoothed particle hydrodynamics", *Science and Technology of Energetic Materials*, **66**(6), 421-424.
- Lancaster, G.M. (1981), "Surfaces generated by moving least squares methods", *Mathematics and Computation*, **3** (37), 141-158.
- Liu, M.B., Liu, G.R. and Lam, K.Y. (2002), "Investigations into water mitigation using a meshless particle method", *Shock Waves*, **12**, 181-195.
- Liu, G.R. and Liu, M.B. (2003), *Smoothed Particle Hydrodynamics*, World Scientific, Singapore.
- Liu, M.B., Liu, G.R. and Lam, K.Y. (2003), "Constructing smoothing functions in smoothed particle hydrodynamics with applications", *J. Comput. Appl. Math.*, **155**, 263-284.
- Liu, M.B., Liu, G.R. and Lam, K.Y. (2003), "A one-dimensional meshfree particle formulation for simulating

- shock waves”, *Shock Waves*, **13**, 201-211.
- Liu, M.B., Liu, G.R., Lam, K.Y. and Zong, Z. (2003), “Smoothed particle hydrodynamics for numerical simulation of underwater explosion”, *Comput. Mech.*, **30**, 106-118.
- Lucy, L.B. (1977), “Numerical approach to testing the fission hypothesis”, *Astronomical J.*, **82**, 1013-1024.
- Masuda, S. and Noguchi, H. (2006), “Analysis of structure with material interface by meshfree method”, *CMES-Comput. Model. Eng. Sci.*, **11**, 131-143.
- Monaghan, J.J. (1992), “Smoothed particle hydrodynamics”, *Annual Review of Astronomical and Astrophysics*, **30**, 543-574.
- Monaghan, J.J. (1994), “Simulating free surface flows with SPH”, *J. Comput. Phys.*, **110**, 399-406.
- Morris, J.P. and Monaghan J.J. (1997), “A switch to reduce SPH viscosity”, *J. Comput. Phys.*, **136**, 41-50.
- Rojek, J. and Oñate, E. (2008), “Multiscale analysis using a coupled discrete/finite element model”, *Interaction and Multiscale Mechanics, An Int. J.*, **1**(1), 1-31.
- Sigalotti, L.D.G., Lopez, H., Donoso, A., Sira, E. and Klapp, J. (2006), “A shock-capturing SPH scheme based on adaptive kernel estimation”, *J. Comput. Phys.*, **212**, 124-149.
- Sod, G.A. (1978), “A survey of several finite difference methods for systems of hyperbolic conservation laws”, *J. Comput. Phys.*, **27**, 1-31.
- Toro, E.F. (1997), *Riemann Solvers and Numerical Methods for Fluid Dynamics - A Practical Introduction*, Springer.